Cerebral Cortex, March 2021;31: 1622–1631

doi: 10.1093/cercor/bhaa314
Advance Access Publication Date: 4 November 2020
Original Article

ORIGINAL ARTICLE

Motion Coherence and Luminance Contrast Interact in Driving Visual Gamma-Band Activity

Franziska Pellegrini[1,2,3,5], David J. Hawellek[1,2,3,4], Anna-Antonia Pape[2,3], Joerg F. Hipp[2,3,4] and Markus Siegel[1,2,3]

[1]Hertie Institute for Clinical Brain Research, University of Tübingen, 72076 Tübingen, Germany, [2]Centre for Integrative Neuroscience, University of Tübingen, 72076 Tübingen, Germany, [3]MEG Center, University of Tübingen, 72076 Tübingen, Germany, [4]Roche Pharma Research and Early Development, Neuroscience and Rare Diseases, Roche Innovation Center Basel, 4070 Basel, Switzerland and [5]Berlin Center for Advanced Neuroimaging, Charité - Universitätsmedizin Berlin, 10117 Berlin, Germany

Address correspondence to Franziska Pellegrini, Charité - Universitätsmedizin Berlin, Charitéplatz 1, 10117 Berlin, Germany.
Email: franziska.pellegrini@charite.de; and Markus Siegel, Centre for Integrative Neuroscience, Otfried-Mueller Strasse 25, 72076 Tübingen, Germany.
Email: markus.siegel@uni-tuebingen.de

Abstract

Synchronized neuronal population activity in the gamma-frequency range (>30 Hz) correlates with the bottom-up drive of various visual features. It has been hypothesized that gamma-band synchronization enhances the gain of neuronal representations, yet evidence remains sparse. We tested a critical prediction of the gain hypothesis, which is that features that drive synchronized gamma-band activity interact super-linearly. To test this prediction, we employed whole-head magnetencephalography in human subjects and investigated if the strength of visual motion (motion coherence) and luminance contrast interact in driving gamma-band activity in visual cortex. We found that gamma-band activity (64–128 Hz) monotonically increased with coherence and contrast, while lower frequency activity (8–32 Hz) decreased with both features. Furthermore, as predicted for a gain mechanism, we found a multiplicative interaction between motion coherence and contrast in their joint drive of gamma-band activity. The lower frequency activity did not show such an interaction. Our findings provide evidence that gamma-band activity acts as a cortical gain mechanism that nonlinearly combines the bottom-up drive of different visual features.

Key words: gain, gamma-band oscillations, luminance contrast, MEG, motion coherence

Introduction

Synchronized neuronal population activity in the gamma-frequency range (>30 Hz), that is, gamma-band activity, is a hallmark of feed-forward visual processing (Donner and Siegel 2011; Vinck et al. 2013; van Kerkoerle et al. 2014; Fries 2015). It is robustly driven by sensory stimulation and varies with several parameters of visual stimuli such as stimulus size (Gieselmann and Thiele 2008; Perry et al. 2013; Vinck and Bosman 2016), luminance contrast (Hall et al. 2005; Henrie and Shapley 2005; Niessing 2005; Ray and Maunsell 2010b; Hadjipapas et al. 2015; Perry et al. 2015), stimulus orientation (Friedman-Hill 2000; Siegel and König 2003; Koelewijn et al. 2011), and visual motion (Liu and Newsome 2006; Siegel et al. 2007; Muthukumaraswamy and Singh 2013). Gamma-band activity increases monotonically with visual motion coherence (Siegel et al. 2007) and increases approximately linearly with luminance contrast (Hall et al. 2005; Henrie and Shapley 2005; Niessing 2005; Ray and Maunsell 2010b; Hadjipapas et al. 2015; Perry et al. 2015). Gamma-band activity is also related to cognitive processes. It correlates with selective visual attention (Fries 2001; Siegel et al. 2008) and predicts visual discrimination performance (Siegel et al.

2008) as well as reaction times during sensory discrimination (Womelsdorf et al. 2006; Rohenkohl et al. 2018).

Gamma-band activity may act as a cortical gain mechanism. Synchronized spikes have a super-additive impact on downstream neurons (MacLeod et al. 1998; Salinas and Sejnowski 2001; Azouz and Gray 2003; Laughlin and Sejnowski 2003; Fries 2009; Donner and Siegel 2011). This impact may be further enhanced by the alignment of rhythmic spiking to the phase of postsynaptic excitability fluctuations (Fries 2005; Siegel et al. 2008). Thus, synchronized gamma-band activity may increase the impact, that is, gain, of neuronal representations (König et al. 1996; Salinas and Sejnowski 2001; Fries et al. 2007; Donner and Siegel 2011; Fries 2015).

A critical prediction of this cortical gain hypothesis is that a combination of visual features that drive gamma-band activity should result in a super-linear (e.g., multiplicative) interaction, rather than a mere additive effect of these features on gamma-band activity. We tested this prediction recording magnetencephalography (MEG) in human participants that viewed dynamic random-dot motion patterns with varying luminance contrast and motion coherence. We found that, in addition to a linear drive of gamma activity through coherence and contrast, these stimulus features indeed showed a multiplicative interaction. Modulations of gamma-band activity were localized to visual cortex and accompanied by a more widespread modulation of lower frequency activity (8–32 Hz) that did not show an interaction between stimulus features. Our results provide novel evidence that gamma-band activity reflects a bottom-up driven cortical gain mechanism.

Material and Methods

Participants

Nineteen subjects (5 male; mean ± SD age, 26.2 ± 3.2 years; age range, 21–35 years) participated in the experiment and received monetary compensation for their participation. The study was conducted in accordance with the Declaration of Helsinki and approved by the local ethics committee, and informed consent was obtained from all subjects prior to the recordings. All subjects were in good health and had normal or corrected-to-normal vision.

Stimuli and Behavioral Task

The stimuli consisted of dynamic random-dot patterns with bright dots on a black background (Fig. 1). During the entire experiment, subjects sat in the MEG in upright position. For every trial, they first saw a blank black screen with a fixation cross in the center (Fig. 1A). After 500 ms, a dynamic random-dot stimulus appeared on either the left or the right side of the fixation cross (10° eccentricity, 12° stimulus diameter). After 1000 ms, the stimulus disappeared. After a variable delay (300–600 ms), a Go cue was given through a brief dimming of the fixation cross (1 frame, ~16 ms). The participants then pressed one of two buttons to indicate whether they saw an upward or downward stimulus motion.

The stimuli had varying features with three levels of motion coherence (12%, 56%, and 100%; Fig. 1B) and three levels of luminance contrast (Weber contrast levels: 20%, 60%, and 100%). The varying coherence was induced using random direction noise with the "same" rule (Scase et al. 1996) (12° stimulus diameter, 1000 dots, 10 deg/s dot speed, 0.1° dot radius). Thus,

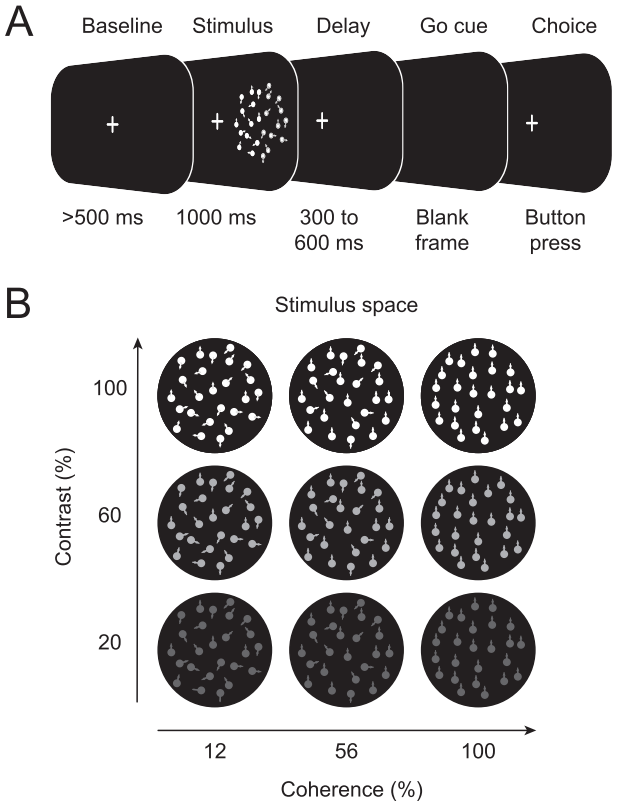

Figure 1. Experimental paradigm and stimulus space. (*A*) On each trial, subjects fixated a small central fixation cross. Following a blank baseline (>500 ms), a dynamic random-dot stimulus appeared either on left or right side and disappeared again after 1000 ms. After a variable delay (300–600 ms), the fixation cross disappeared as a go cue for the response. Subjects reported the perceived motion direction (up vs. down) with a button press (left vs. right hand). (*B*) Stimuli varied in motion coherence (12%, 56%, and 100%) and luminance contrast (20%, 60% and 100%).

a fraction of "signal dots" moved all in the same signal direction (upward or downward movement) during the entire stimulus presentation, while another fraction of "noise dots" moved in random directions. We manipulated the contrast of the stimuli by increasing dot brightness against a constant luminance background. The task factors motion direction (upward vs. downward), presentation side (left vs. right), coherence level, and contrast level were counter-balanced and randomly varied across trials during every experiment. The stimulus–response mapping (button press with the left vs. right hand to indicate upward vs. downward motion, respectively) was counter-balanced across subjects.

Sixteen subjects participated in the full experiment of 900 trials: one subject stopped after 283 trials, one subject stopped after 798 trials, and one subject after 894 trials. This study focused on neuronal correlates of visual stimulus features rather than of behavior. Thus, the behavioral task was designed such that, except for the lowest motion coherence, the subjects' performance was nearly perfect: 12% coherence: 62% (±9% SD) correct performance; 56% coherence: 92% (±7% SD) correct performance; and 100% coherence: 98% (±2% SD) correct performance. Likewise, the median reaction time showed a ceiling effect for higher coherence levels: 12% coherence: 522 ms (±328 ms SD); 56% coherence: 457 ms (±281 ms SD); and 100% coherence: 453 ms (±276 ms SD).

Data Acquisition and Preprocessing

MEG was continuously recorded using a 275-channel whole-head system (Omega 2000, CTF Systems Inc.) in a magnetically shielded room. The head position relative to the sensors was measured using three head localization coils (nasion, left/right pre-auricular points). Electroencephalography (EEG) recordings were performed in parallel to the MEG recordings. The EEG data are not presented here. The MEG signals were recorded with a sampling rate of 2483.8 Hz.

All analyses were performed in Matlab (MathWorks) using custom code and the open source toolboxes Fieldtrip (Oostenveld et al. 2011) and SPM12 (http://www.fil.ion.ucl.ac.uk/spm). Off-line, the data were high-pass filtered with a cut-off frequency of 1 Hz and down-sampled to 500 Hz. Line noise was removed by applying band-stop filters at 50, 100, 150, 200, and 250 Hz with cut-offs at 1 Hz (all fourth-order zero-phase Butterworth filters). Trials containing jumps and channels that were affected from flux trapping due to the simultaneous EEG–MEG recordings were excluded from the analysis. We conducted an independent component analysis (FAST ICA; Hyvärinen and Oja 2000) to further clean the data from eye blink, eye movement, muscular, and pulse artefacts. We inspected the first 100 components of each subject visually according to their topology, time courses, and spectra. Components that could be clearly detected as artefacts were subtracted from the data before further analysis (mean: 4.7; SD: 4.1 components per subject).

During the MEG recordings, we performed noncontact infrared-based eye-tracking in 18 out of 19 subjects.

Spectral Analyses

All spectral analyses were performed using Morlet's wavelets (Tallon-Baudry et al. 1996). We computed the time–frequency representation (TFR) for frequency f of the signal $x(t)$ at time t with the convolution operation

$$\mathrm{TFR}(t,f) = x(t) * w(t,f). \quad (1)$$

We write $w(t,f)$for Morlet's wavelets

$$w(t,f) = Ae^{-t^2/2\sigma_t^2} e^{i2\pi ft}, \quad (2)$$

where σ_t is the standard deviation (SD) of the signal in the time domain and A is a normalization factor. In both time and frequency domains, Morlet's wavelets are Gaussian shaped. $\sigma_f = f/q$ is the SD in the frequency domain at frequency f and q is the width of the wavelet. The SD in the time domain is given by $\sigma_t = 1/(2\pi\sigma_f)$. We set $q = 5$ and estimate TFR(t,f) at frequencies between 8 and 256 Hz, logarithmically scaled in quarter octave steps. Finally, we subsampled TFR(t,f) in the time-domain with a step-size of 20 ms.

Source Localization

We projected the frequency-decomposed MEG data to predefined source locations using adaptive linear spatial filters (Beamforming; Van Veen et al. 1997; Gross et al. 2001). To account for different head anatomy, we constructed a personalized lead field for each participant. The lead field describes the signal measured at the sensor-level for an isolated dipole with fixed current pointing to each of the 3 principle axes (forward model). The computation of lead fields was based on head models generated from T_1 magnetic resonance imaging (MRI) data of each subject. First, we segmented the MRI data into different tissue types: gray and white matter, cerebrospinal fluid, skull, and skin. Based on the segmented MRI data, we constructed individual single-shell head models (Nolte 2003) and subsequently nonlinearly registered a standardized source model to the individual brain shapes (Hipp et al. 2012). The source model contained 457 locations that homogeneously covered the space below the MEG sensors ~7 mm beneath the skull. Source coordinates, head model, and MEG channels were calculated relative to the three head localization coils. We used DICS beamforming in the frequency domain (Gross et al. 2001) to project the data from sensor level to source space. Beamforming renders activity from sources of interest with unit gain while maximally suppressing contribution from all other sources. Briefly, for every frequency f, DICS beamforming uses the sensor-level cross-spectral density matrix (CSD) and the individual lead fields L to define spatial filters F

$$F(i,f) = \left[L(i,f)^{\mathrm{T}}\ \mathrm{CSD}_{\mathrm{real}}(f)^{-1}\ L(i,f)\right]^{-1} L(i,f)^{\mathrm{T}}\ \mathrm{CSD}_{\mathrm{real}}(f)^{-1}, \quad (3)$$

where i denotes sources and $\mathrm{CSD}_{\mathrm{real}}$ is the real part of the CSD. To obtain the 3-by-3 source level CSD (CSD_i), we projected the sensor level CSD through the filter F

$$\mathrm{CSD}_i(f) = \mathrm{real}\left(F(i,f)\ \mathrm{CSD}(f) F(i,f)^{\mathrm{T}}\right). \quad (4)$$

For every frequency f, we then performed principal component analysis (singular value decomposition) on the source level $\mathrm{CSD}_i(f)$ and selected the first principal component that represents the most dominant dipole orientation. Subsequently, we projected the Filter F onto the first principal component and obtained F_{pri}. Finally, we projected the TFR data from the sensor level to source level by multiplying them with the filter F_{pri}

$$\mathrm{TFR}_i(t,f) = F_{\mathrm{pri}}(i,f)\ \ \mathrm{TFR}(t,f), \quad (5)$$

where TFR_i denotes the time–frequency representation on the source-level.

Response Normalization

To suppress stimulus-evoked responses phase-locked to stimulus onset, we subtracted the average potential across trials per condition, subject, time–frequency bin, and source.

To project the data into a consistent relationship between cortical hemisphere and side of stimulation (left vs. right), we flipped the responses across the sagittal axis of the brain such that the left hemisphere of the brain represented activity contralateral to the stimulation and the right hemisphere represented the activity ipsilateral to the stimulation.

We characterized spectral responses $R(f)$ as the percentage of change in signal power at frequency f and time t relative to the prestimulus baseline

$$R(f) = \frac{S(f) - B(f)}{B(f)} * 100, \quad (6)$$

where $S(f)$ denotes the spectral power in the temporal interval of interest and $B(f)$ denotes the spectral power during the prestimulus baseline (500 ms before up to stimulus onset), averaged across all trials and conditions. We analyzed the spatial distribution of power relative to baseline in five frequency bands, averaged across all subjects, trials, and time bins from 0.1 to 1.1 s poststimulus onset. In particular at later time points, we observed activity modulations that localized to the motor cortex, which likely reflected neuronal process related to response preparation. Motor preparation and a potential decrease of visual attention during the late stimulus interval may in particular occur for stimuli with higher motion coherence, which allow for early response preparation. Thus, to avoid any potential confounds from such an effect, we restricted all analyses to the early time window from 0.1 to 0.6 s poststimulus onset. In order to assess the modulation of neuronal responses by stimulus conditions (see below), we normalized responses by the mean across all trials and conditions for each subject, time, frequency, and source bin. We used cluster-based permutation statistics to test for significant changes of power relative to baseline (Fig. 2). We determined cluster sizes of contiguous differences from zero with identical sign with $P < 0.05$ (random effects two-tailed t-test, uncorrected). Before cluster definition, we applied a neighborhood filtering (filter parameter: 0.5) to remove spurious bridges between clusters (Hipp et al. 2011). The analysis was repeated 10 000 times, shuffling the signs of the effects per subject and taking the maximum cluster size determined as above for each shuffle. A cluster was determined to be significant at $P < 0.05$ when its size exceeded the 95th percentile of this maximum cluster size distribution (Nichols and Holmes 2002).

Analysis of Response Modulation

The neuronal response y was modeled as a combination of predictor variables x_1(contrast) and x_2 (motion coherence)

$$y = \beta_0 + \beta_1 x_1 + \beta_2 x_2 + \beta_3 x_1 x_2 + \beta_4 x_1^2 + \beta_5 x_2^2 + \beta_6 x_1^2 x_2^2 \quad (7)$$

with β reflecting the polynomial coefficients. To assess the amount of variance that each predictor accounted for independently, we orthogonalized the regressors prior to model fitting using QR-decomposition. For the spectrally, temporally, and spatially resolved analyses (Fig. 3), we fitted the response model for each subject. We then used the same cluster-based permutation statistics as for the power response to test for significant model coefficients.

For the analysis of response modulation for fixed spectro-temporal windows on the population level (Fig. 4), we fitted one response model to the data of all subjects. We then used sequential polynomial regression (Büchel et al. 1998; Rees et al. 2000; Siegel et al. 2007) to assess the modulation of responses by contrast and coherence. Starting with the zero-order (constant) model and based on F-statistics (Draper and Smith 1998), we tested whether incrementally adding new predictors improves the model significantly ($P < 0.05$). We assessed the confidence interval (CI) around the respective β-weights by conducting a bootstrap analysis with 1000 iterations. In each iteration, we randomly drew a subset of 19 subjects (with repetition) out of the complete set of 19 subjects and calculated the coefficients based on this subset. The CIs represent the 2.5th and 97.5th percentile of the resulting distribution. We applied leave-one-out cross-validation across subjects to account for overfitting.

Control Analyses

In a first control analysis, we investigated a potential confound due to eye movements. We compared the variance of eye movements (0.1 to 0.6 s poststimulus onset) among the three levels of motion coherence and contrast (pairwise sign-rank test). We stratified the data to equate eye movements across different levels of motion coherence and contrast. For each subject, we randomly left out trials for the lowest and highest contrast level such that the median of eye movements for these levels moved closer to the median of eye movements for the mean contrast level. We repeated this removal until the median eye movements were equated across contrast levels. We then performed the same stratification procedure for motion-coherence levels and performed the polynomial regression analysis on the stratified data.

In a second control analysis, we repeated the polynomial regression analysis for a larger region of interest that included most of contralateral visual cortex.

Results

We recorded MEG in human subjects ($n = 19$) that viewed dynamic random-dot stimuli with varying luminance contrast (3 levels) and motion coherence (3 levels; Fig. 1B). After stimulus presentation (1000 ms) and a variable 300–600 ms delay, the participants indicated whether they saw an upward or a downward motion with a button press (Fig. 1A).

We source-reconstructed the MEG data at 457 locations that homogeneously covered the cerebral cortex about 7 mm below the skull. In line with previous findings (Hall et al. 2005; Siegel et al. 2007; Hipp et al. 2011), stimulus presentation increased gamma-band activity (>64 Hz) compared with the blank fixation baseline in the visual cortex contralateral to the visual stimulus (Fig. 2A; both $P < 0.01$, cluster-based permutation). The robust increase in the gamma band was accompanied by a more widespread decrease in lower frequency bands (Fig. 2A; all three frequency bands between 8 and 64 Hz $P < 0.01$, cluster-based permutation).

For all further analyses, we averaged responses across the 5% sources within the strongest gamma-band response, which were located in contralateral occipital visual cortex (Fig. 2B inset). Furthermore, we restricted the analysis to the early interval from 0.1 to 0.6 s poststimulus onset to discount potential confounds due to response preparation at later timepoints. Both, the high-frequency enhancement and low-frequency suppression in visual cortex started around 0.1 s poststimulus onset and were then sustained (Fig. 2B; both $P < 0.01$, cluster-based permutation).

We next addressed how gamma-band activity varied with luminance contrast and motion coherence (Fig. 2C). For all 3 levels of motion coherence and contrast, visual stimulation induced a robust increase of gamma-band activity and decrease of low-frequency activity (Fig. 2C; all clusters $P < 0.05$, cluster-based permutation). Furthermore, gamma-band activity increased monotonically with both visual features (Fig. 2C). We next quantitatively assessed these modulations and tested for

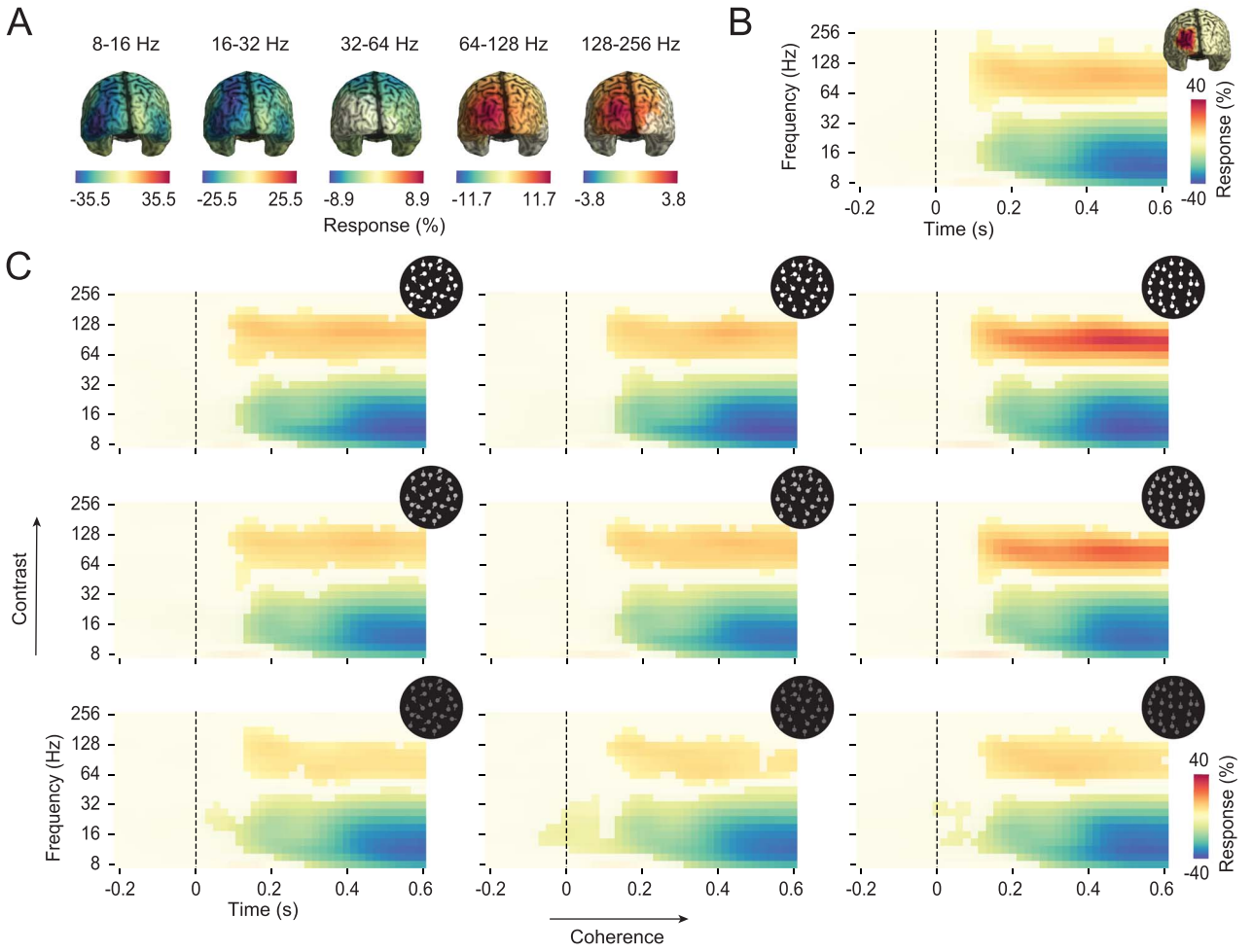

Figure 2. Stimulus-induced responses relative to baseline. (*A*) Cortical distribution of the power response during stimulation (0.1–1.1 s) in five frequency bands. Brains are viewed from the back. (*B*) Power response resolved in time and frequency in occipital cortex contralateral to the visual hemifield of stimulation. The region of interest is depicted on the upper right. (*C*) Time–frequency resolved power responses in each stimulus condition. In all panels, statistical significance ($P < 0.05$ corrected, cluster permutation) is indicated by color opacity. Same color scale as in (*B*).

a potential interaction between coherence and contrast using a model-based approach.

We performed sequential polynomial regression to model the neuronal response as a linear and quadratic function of motion coherence and luminance contrast as well as of the interaction of these linear and quadratic features (Büchel et al. 1998; Rees et al. 2000; Siegel et al. 2007). The fitted model coefficients reveal the corresponding linear and quadratic modulations of the neuronal response by coherence and contrast (Fig. 3A). Importantly, stimulus coherence and contrast were uncorrelated by design, and all model coefficients were estimated independently using orthogonalized regressors. Thus, the interaction coefficients reflect multiplicative response modulations that cannot be explained by linear modulations (see Materials and Methods for further details).

We found that both contrast and motion coherence had a positive linear effect on visual gamma-band activity (Fig. 3A; contrast: $P < 0.01$; coherence: $P < 0.0001$, cluster-based permutation). These modulations were confined to frequencies from about 64 to 128 Hz, started shortly after stimulus onset and were then sustained throughout the stimulation period. In addition and in agreement with previous results (Gray and Singer 1989; Siegel and König 2003; Siegel et al. 2007), we observed a linear decrease of activity with contrast and coherence at lower frequencies from about 8 to 25 Hz ($P < 0.05$, cluster-based permutation). The contrast effect became significant around 150 ms after stimulus onset; the coherence effect became significant after 350 ms after stimulus onset. There was a weak sub-linear (negative quadratic) modulation of gamma-band activity with contrast ($P < 0.05$, cluster-based permutation). In addition and in line with previous results (Siegel et al. 2007), we observed a significant supra-linear (quadratic) increase of gamma-band activity with motion coherence between 32 and 128 Hz ($P < 0.001$, cluster-based permutation).

Consistent with our main hypothesis, we also found a robust multiplicative interaction between coherence and contrast ($P < 0.01$, cluster-based permutation, Fig. 3A). This interaction was confined to the frequency range between 64 and 128 Hz, became significant around 200 ms after stimulus onset, and was then sustained. There was no such interaction between the negative response modulation of coherence and contrast at lower frequencies.

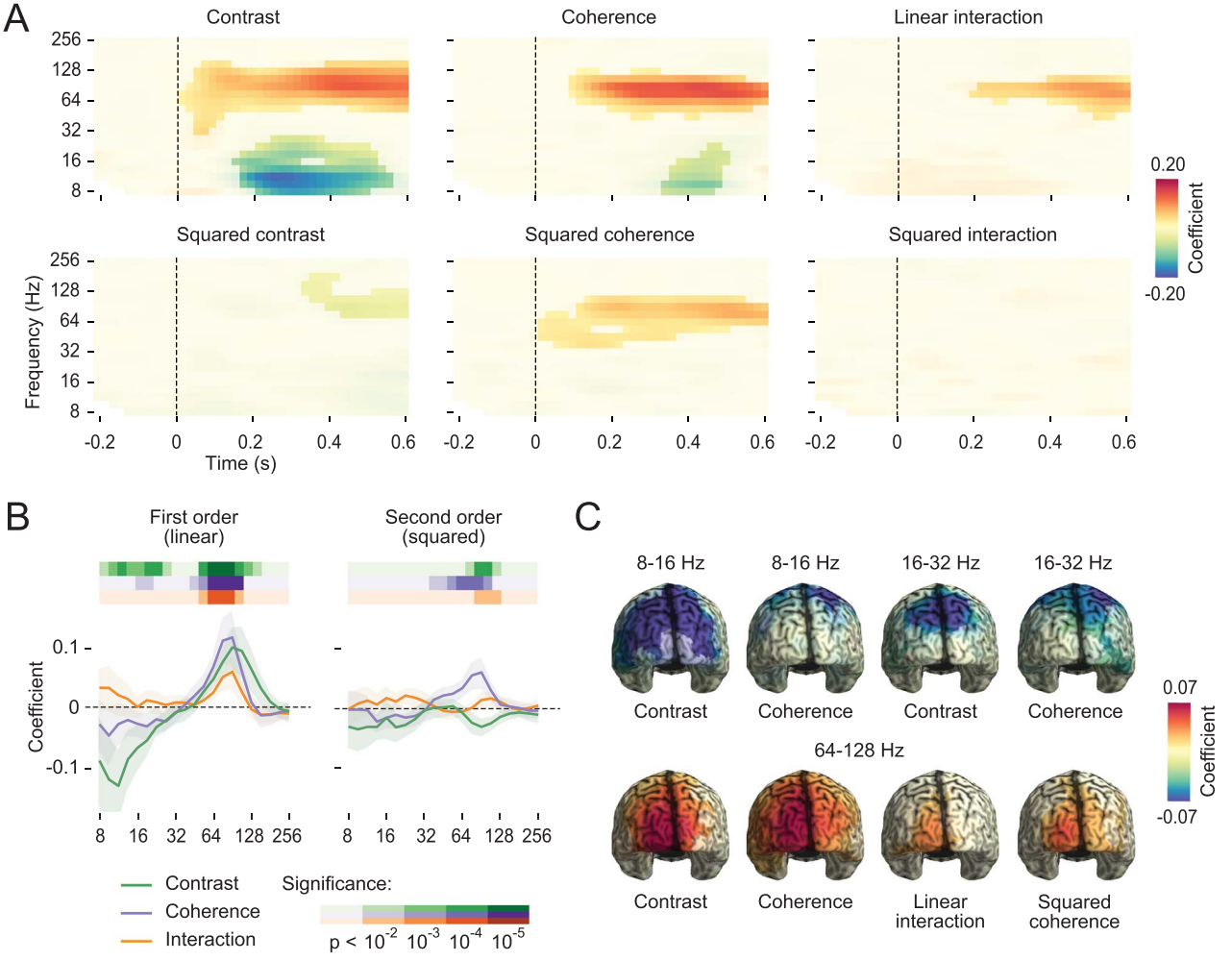

Figure 3. First-order (linear) and second-order (quadratic) response modulation by luminance contrast and motion coherence. (*A*) Results of a sequential polynomial regression per time–frequency bin, including first- and second-order coefficients and their interactions. Statistical significance ($P < 0.05$ corrected, cluster permutation) is indicated by color opacity. Contralateral occipital cortex. (*B*) Response coefficients as a function of frequency for the time window from 0.1 to 0.6 s paststimulus onset. Shaded areas represent the 95% confidence intervals. Significant deviations from zero are indicated by the colored bars above the line plots. Contralateral occipital cortex. (*C*) Spatial specificity of selected response modulations in the time window from 0.1 to 0.6 s paststimulus onset. Statistical significance ($P < 0.05$ corrected, cluster permutation) is indicated by color opacity. See Supplementary Figure 1 for cortical distributions of all factors for all frequency bands.

To further investigate the spectral profile of response modulations through coherence and contrast, we applied the same stepwise modeling (sequential polynomial regression) to the stimulus response averaged across time (0.1 to 0.6 s poststimulus onset) at each single frequency (Fig. 3B). In line with the temporally resolved analysis, this approach revealed robust linear effects of contrast and motion coherence in the gamma band and lower frequency ranges as well as quadratic effects of both visual features in the gamma band (all $P < 0.01$, cluster-based permutation). We observed a multiplicative interaction between coherence and contrast in the gamma band. Furthermore, in this analysis, we also observed a weak second-order interaction of contrast and coherence for the gamma band ($P < 0.05$; multiplicative interaction of quadratic coherence and contrast). There was no significant linear or quadratic interaction of coherence and contrast for lower frequency ranges.

In which cortical regions do visual contrast and coherence modulate frequency-specific neuronal population activity? To answer this question, we repeated the above analyses for each source location across the entire cortex, for 5 frequency bands (8–16, 16–32, 32–64, 64–128, and 128–256 Hz) in the time range of 0.1 to 0.6 s poststimulus and applied a spatial cluster-permutation statistic (Fig. 3C, 0.1 to 0.6 s poststimulus; all factors and frequency ranges that are presented show significant clusters at $P < 0.05$, cluster-based permutation; see Supplementary Fig. 1 for all factors and frequency ranges). Contrast and coherence induced a negative linear modulation in low frequencies (8–32 Hz) that extended along the dorsal visual stream peaking in occipitoparietal regions. The linear gamma-band modulations of contrast and coherence, including their multiplicative interaction, were more confined and shifted toward the pole of the occipital cortex.

In a final step, we investigated how well the polynomial model fit the data. To this end, we repeated the regression analysis for neuronal responses in five frequency bands (Fig. 4; 0.1 to 0.6 s poststimulus; responses in contralateral visual cortex as above). Models of all but the middle frequency band (32–64 Hz) included contrast as a linear predictor (all $P < 0.001$). Models

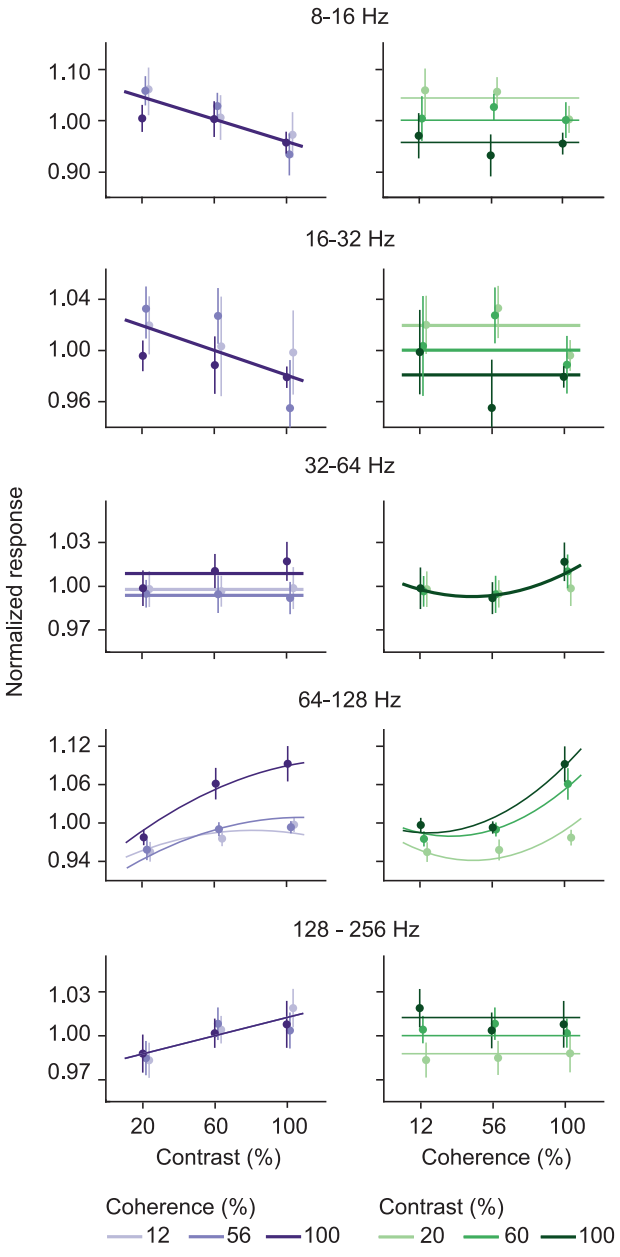

Figure 4. Average power response in the time window from 0.1 to 0.6 s in contralateral occipital cortex and fitted response models as a function of contrast, coherence, and frequency band. Dots and error bars indicate the mean response and the corresponding 95% confidence interval across subjects. Lines indicate the fitted polynomial response model. Models include the significant coefficients ($P < 0.05$) of the sequential polynomial regression for the respective frequency band. Please note that the fits are displayed in the original nonorthogonalized contrast- and coherence-space to enhance readability. Plots were slightly displaced on the x-axis to avoid data overlap and enhance readability.

between 32 and 128 Hz also included a linear coherence predictor (all $P < 0.05$). The models between 32 and 128 Hz included squared coherence (both $P < 0.05$), and for 64–128 Hz, the model included quadratic contrast ($P < 0.05$). Importantly, the linear interaction of coherence and contrast only improved the model for 64–128 Hz ($P < 0.0001$). For this frequency range (64–128 Hz), the full response model including linear contrast ($ß = 0.34$, 95% CI = [0.23,0.45]), linear coherence ($ß = 0.36$, CI = [0.26,0.47]), their interaction ($ß = 0.16$, CI = [0.09,0.22]), as well as quadratic contrast ($ß = -0.08$, CI = [−0.13,-0.03]) and quadratic coherence ($ß = 0.18$, CI = [0.11,0.25]). We performed a leave-one-out cross-validation analysis to quantitatively assess the model fit. For 64–128 Hz, the polynomial model including the linear interaction of coherence and contrast well fit the neuronal response ($R^2 = 0.54$). Furthermore, in accordance with the stepwise-regression analysis, leaving out the interaction term of the model in the cross-validation analysis resulted in a reduced model fit ($R^2 = 0.50$).

Different levels of motion coherence or contrast may lead to different eye movements. Indeed, a control analysis revealed significantly stronger eye movements (eye position variance, 0.1 to 0.6 s poststimulus onset) for stimuli with higher motion coherence (100% vs. 56% coherence, $P < 0.05$, sign-rank test) and higher contrast (all pairwise comparisons $P < 0.001$, sign-rank test). To rule out that these differences in eye movements confounded our results, we repeated our main analysis after stratifying the data to equate eye movements across levels of motion coherence and contrast (trials omitted: 214 mean ± 152 SD across subjects). The results of this control analysis were very similar to the above findings (Supplementary Fig. 2). Most importantly, the linear interaction between motion coherence and contrast for the gamma band (64–128 Hz) was also significant for the stratified data ($P < 0.0001$). We thus concluded that this interaction was not confounded by eye movements.

In a second control analysis, we investigated if our key results depended on the particular choice of cortical region of interest. We repeated the analyses with a larger region of interest including most of contralateral visual cortex (Supplementary Fig. 3). This control analysis yielded largely the same results as the above analyses that were based on the smaller region of interest. Most importantly, also for this control analysis revealed a significant linear interaction between motion coherence and contrast for the gamma band (64–128 Hz, $P < 0.001$).

Discussion

Here, we combined MEG, source reconstruction, and parametric visual stimulation to test a critical prediction of the hypothesis that visual gamma-band activity acts as a cortical gain mechanism, which is that features that drive gamma-band activity interact super-linearly. To this end, we investigated the joined effect of visual contrast and motion coherence on gamma-band activity in human visual cortex. We found wide-spread activity modulations along the visual hierarchy in response to varying contrast and motion coherence. Low-frequency activity (8–32 Hz) decreased with coherence and contrast along the dorsal visual stream but exhibited no interaction between stimulus features. In contrast, for gamma-band activity, the driving influences of contrast and coherence interacted multiplicatively, thus confirming the prediction for a gain mechanism. Our findings provide a novel evidence for the notion of gamma-band activity as a signature of local interactions that is driven through bottom-up sensory features and that regulates the gain or impact of sensory processing onto downstream regions (Siegel et al. 2007, 2008, 2012; Fries 2015).

The influence of contrast on neuronal spiking activity in visual cortex has been studied extensively. Neurons in areas along the dorsal visual stream exhibit a sigmoidal contrast response function (Albrecht and Hamilton 1982; Sclar et al. 1990; Martínez-Trujillo and Treue 2002), with different cells saturating at different contrast levels (Albrecht and Hamilton 1982).

Gamma-band activity has been reported to increase approximately linearly with contrast in human MEG and EEG (Hall et al. 2005; Hadjipapas et al. 2015; Perry et al. 2015), while both linear (Logothetis et al. 2001; Henrie and Shapley 2005) and saturating (sub-linear; Ray and Maunsell 2010; Hadjipapas et al. 2015) modulations have been observed invasively in monkey visual cortex. In accordance with these reports, we found that gamma-band activity increased monotonically with contrast. Furthermore, we found that the increase of gamma-band activity with contrast was saturating (sub-linear), which accords well with recent results in nonhuman primates (Ray and Maunsell 2010b; Hadjipapas et al. 2015). We did not observe an accelerating portion of a sigmoidal response function as seen in neural activity or BOLD signals at low contrasts. This could be due to the relatively high contrast values starting from 20% and due to the low resolution with only three contrast levels for the present study.

Previous studies observed a strong relationship between the peak frequency of gamma-band activity and luminance contrast using grating stimuli (Ray and Maunsell 2010b; Hadjipapas et al. 2015). We did not observe such a frequency modulation in the present data (see Fig. 2). This may point to a stimulus specific origin of contrast-dependent frequency shifts in gamma-band activity (gratings vs. random-dot motion).

For motion coherence, response curves are also similar between single unit spiking and gamma-band population activity. The relationship between the motion coherence of a dynamic random-dot pattern and a cell's response is predominantly linear (Britten et al. 1993; Heuer and Britten 2007). Also gamma-band activity in the human MEG increases approximately linearly with the motion coherence of dynamic random-dot patterns, with some subjects showing a quadratic (supra-linear) response (Siegel et al. 2007). Our results confirm these findings with both linear and quadratic modulations of gamma-band activity by motion coherence.

Although the relationship between single stimulus features and gamma-band activity has been studied extensively, little is known about the interaction of different stimulus features. Our results show that two stimulus features that monotonically increase gamma-band activity (contrast and motion coherence) interact supra-linearly in human visual cortex. This finding accords well with another MEG study that investigated the effect of three different stimulus parameters on gamma-band activity (full-field vs. quadrant, static vs. motion, circular vs. linear grating; Muthukumaraswamy and Singh 2013). Gamma activity exhibited main effects for all three stimulus features and, in accordance with the present results, also significant positive interactions among all factors (Muthukumaraswamy and Singh 2013). These and our findings contrast with another recent fMRI study (Birman and Gardner 2018), which did not find a significant interaction between motion coherence and contrast for dynamic random dot patterns.

Local gamma-band activity likely arises from the interplay of both lateral excitatory interactions and local inhibitory feedback (Bush and Sejnowski 1996; Kopell et al. 2000; Siegel et al. 2000; Bartos et al. 2007; Fries et al. 2007; Cardin et al. 2009; Fries 2009; Sohal et al. 2009; Donner and Siegel 2011; Vinck and Bosman 2016). The increase of gamma-band activity with contrast and motion coherence may reflect the enhanced rhythmic structuring of spiking activity with enhanced recruitment of these locally recurrent interactions through stronger bottom-up drive. Furthermore, stronger motion coherence enhances the spatiotemporal predictability of visual stimuli, which may further enhance the recruitment of stimulus specific lateral excitation (Gilbert and Wiesel 1989; Lund et al. 2003) and inhibition (Coen-Cagli et al. 2015; Vinck and Bosman 2016).

Visual gamma-band activity increases with selective visual attention (Fries 2001; Siegel et al. 2008) and enhances perceptual accuracy (Siegel et al. 2008) and response speed (Womelsdorf et al. 2006). Several factors may contribute to these behavioral effects. On the one hand, local gamma-band activity may rhythmically modulate and enhance the information content of neuronal spiking (Siegel et al. 2009; Womelsdorf et al. 2012; Vinck and Bosman 2016). On the other hand, local gamma-band activity may enhance the impact or gain of spiking activity on subsequent processing stages by two distinct mechanisms. First, the temporal synchronization of presynaptic spikes likely leads to their super-additive impact on postsynaptic neurons (MacLeod et al. 1998; Salinas and Sejnowski 2001; Azouz and Gray 2003; Laughlin and Sejnowski 2003; Fries 2009; Donner and Siegel 2011). Second, the rhythmic synchronization of presynaptic spiking may enhance its downstream impact by enabling its phase-alignment to corresponding postsynaptic rhythmic excitability fluctuations (Fries 2005; Siegel et al. 2008; Gregoriou et al. 2009; Bosman et al. 2012; Grothe et al. 2012). Our findings support this notion by showing a multiplicative interaction, that is, an enhanced gain of gamma-band responses among visual features that drive this type of neuronal population activity.

Notably, we did not observe an interaction of coherence and contrast in their modulation of low-frequency activity (<30 Hz). Although both features monotonically suppressed low-frequency activity in a graded fashion, there was no interaction between these effects. While ample evidence supports a behavioral effect of visual low-frequency population activity in particular in the alpha band (Thut et al. 2006; Siegel et al. 2008; Jensen and Mazaheri 2010), our results suggest that, in contrast to gamma band, slow rhythmic population activity may not exert a gain-like interaction between different visual features.

An interesting question is whether the different stimulus features modulated gamma-band activity preferentially in different cortical areas. Contrast may be expected to preferentially modulate earlier processing stages with steep contrast–response functions (e.g., V1), while motion coherence may preferentially modulate later stages specialized in motion processing, such as area MT+ (Becker et al. 2008; Birman and Gardner 2018). Such differences may contribute to the multiplicative interaction in average gamma activity across visual cortex through a sequential gain enhancement across several processing stages. Although we observed modulations of gamma-band activity specifically in the contralateral visual cortex, due to the limited spatial resolution, it is difficult to pinpoint the exact cortical stages of gain modulation and interactions with MEG. Further invasive studies are required to address this question.

In sum, we find that visual motion and contrast interact multiplicatively in their drive of visual gamma-band activity. Gamma-band activity may reflect a cortical gain mechanism that combines sensory features and regulates the impact of sensory processing onto downstream regions.

Supplementary Material

Supplementary material is available at *Cerebral Cortex* online.

Notes

Conflict of Interest: J.H. and D.J.H. are full-time employees of F. Hoffmann-La Roche Ltd AAP is a full-time employee of TWT GmbH. The remaining authors declare that the research was conducted in the absence of any commercial or financial relationships that could be construed as a potential conflict of interest.

Funding

European Research Council (ERC) StG335880 (to M.S.); Centre for Integrative Neuroscience (DFG, EXC 307 to M.S.).

Author Contributions

Conceptualization: M.S.; Methodology: F.P., A.A.P., J.F.H., D.J.H., M.S.; Investigation: A.A.P., J.F.H.; Formal Analysis: F.P., D.J.H.; Writing—Original Draft, Review and Editing: F.P., D.J.H., M.S.; Funding Acquisition and Resources: M.S.; Supervision: M.S.

References

Albrecht DG, Hamilton DB. 1982. Striate cortex of monkey and cat: contrast response function. *J Neurophysiol*. 48:217–237.

Azouz R, Gray CM. 2003. Adaptive coincidence detection and dynamic gain control in visual cortical neurons in vivo. *Neuron*. 37:513–523.

Bartos M, Vida I, Jonas P. 2007. Synaptic mechanisms of synchronized gamma oscillations in inhibitory interneuron networks. *Nat Rev Neurosci*. 8:45–56.

Becker HGT, Erb M, Haarmeier T. 2008. Differential dependency on motion coherence in subregions of the human MT+ complex. *Eur J Neurosci*. 28:1674–1685.

Birman D, Gardner JL. 2018. A quantitative framework for motion visibility in human cortex. *J Neurophysiol*. 120:1824–1839.

Bosman CA, Schoffelen J-M, Brunet N, Oostenveld R, Bastos AM, Womelsdorf T, Rubehn B, Stieglitz T, De Weerd P, Fries P. 2012. Attentional stimulus selection through selective synchronization between monkey visual areas. *Neuron*. 75:875–888.

Britten KH, Shadlen MN, Newsome WT, Movshon JA. 1993. Responses of neurons in macaque MT to stochastic motion signals. *Vis Neurosci*. 10:1157–1169.

Büchel C, Holmes AP, Rees G, Friston KJ. 1998. Characterizing stimulus–response functions using nonlinear regressors in parametric fMRI experiments. *Neuro Image*. 8:140–148.

Bush P, Sejnowski T. 1996. Inhibition synchronizes sparsely connected cortical neurons within and between columns in realistic network models. *J Comput Neurosci*. 3:91–110.

Cardin JA, Carlen M, Meletis K, Knoblich U, Zhang F, Deisseroth K, Tsai LH, Moore CI. 2009. Driving fast-spiking cells induces gamma rhythm and controls sensory responses. *Nature*. 459:663–667.

Coen-Cagli R, Kohn A, Schwartz O. 2015. Flexible gating of contextual influences in natural vision. *Nat Neurosci*. 18:1648–1655.

Donner TH, Siegel M. 2011. A framework for local cortical oscillation patterns. *Trends Cogn Sci*. 15:191–199.

Draper NR, Smith H. 1998. Applied regression analysis: includes disk. 3rd ed., *Wiley series in probability and statistics Texts and references section*. New York: Wiley.

Friedman-Hill S. 2000. Dynamics of striate cortical activity in the alert macaque: I. incidence and stimulus-dependence of gamma-band neuronal oscillations. *Cereb Cortex*. 10:1105–1116.

Fries P. 2001. Modulation of oscillatory neuronal synchronization by selective visual attention. *Science*. 291:1560–1563.

Fries P. 2005. A mechanism for cognitive dynamics: neuronal communication through neuronal coherence. *Trends Cogn Sci*. 9:474–480.

Fries P. 2009. Neuronal gamma-band synchronization as a fundamental process in cortical computation. *Annu Rev Neurosci*. 32:209–224.

Fries P. 2015. Rhythms for cognition: communication through coherence. *Neuron*. 88:220–235.

Fries P, Nikolić D, Singer W. 2007. The gamma cycle. *Trends Neurosci*. 30:309–316.

Gieselmann MA, Thiele A. 2008. Comparison of spatial integration and surround suppression characteristics in spiking activity and the local field potential in macaque V1. *Eur J Neurosci*. 28:447–459.

Gilbert CD, Wiesel TN. 1989. Columnar specificity of intrinsic horizontal and corticocortical connections in cat visual cortex. *J Neurosci*. 9:2432–2442.

Gray CM, Singer W. 1989. Stimulus-specific neuronal oscillations in orientation columns of cat visual cortex. *Proc Natl Acad Sci*. 86:1698–1702.

Gregoriou GG, Gotts SJ, Zhou H, Desimone R. 2009. High-frequency, long-range coupling between prefrontal and visual cortex during attention. *Science*. 324:1207–1210.

Gross J, Kujala J, Hamalainen M, Timmermann L, Schnitzler A, Salmelin R. 2001. Dynamic imaging of coherent sources: studying neural interactions in the human brain. *Proc Natl Acad Sci*. 98:694–699.

Grothe I, Neitzel SD, Mandon S, Kreiter AK. 2012. Switching neuronal inputs by differential modulations of gamma-band phase-coherence. *J Neurosci*. 32:16172–16180.

Hadjipapas A, Lowet E, Roberts MJ, Peter A, De Weerd P. 2015. Parametric variation of gamma frequency and power with luminance contrast: a comparative study of human MEG and monkey LFP and spike responses. *Neuro Image*. 112:327–340.

Hall SD, Holliday IE, Hillebrand A, Singh KD, Furlong PL, Hadjipapas A, Barnes GR. 2005. The missing link: analogous human and primate cortical gamma oscillations. *Neuro Image*. 26:13–17.

Henrie JA, Shapley R. 2005. LFP power spectra in V1 cortex: the graded effect of stimulus contrast. *J Neurophysiol*. 94:479–490.

Heuer HW, Britten KH. 2007. Linear responses to stochastic motion signals in area MST. *J Neurophysiol*. 98:1115–1124.

Hipp JF, Engel AK, Siegel M. 2011. Oscillatory synchronization in large-scale cortical networks predicts perception. *Neuron*. 69:387–396.

Hipp JF, Hawellek DJ, Corbetta M, Siegel M, Engel AK. 2012. Large-scale cortical correlation structure of spontaneous oscillatory activity. *Nat Neurosci*. 15:884–890.

Hyvärinen A, Oja E. 2000. Independent component analysis: algorithms and applications. *Neural Netw*. 13:411–430.

Jensen O, Mazaheri A. 2010. Shaping functional architecture by oscillatory alpha activity: gating by inhibition. *Front Hum Neurosci*. 4:186.

Koelewijn L, Dumont JR, Muthukumaraswamy SD, Rich AN, Singh KD. 2011. Induced and evoked neural correlates of orientation selectivity in human visual cortex. *Neuro Image*. 54:2983–2993.

König P, Engel AK, Singer W. 1996. Integrator or coincidence detector? The role of the cortical neuron revisited. *Trends Neurosci*. 19:130–137.

Kopell N, Ermentrout GB, Whittington MA, Traub RD. 2000. Gamma rhythms and beta rhythms have different synchronization properties. *Proc Natl Acad Sci U S A*. 97:1867–1872.

Laughlin SB, Sejnowski TJ. 2003. Communication in neuronal networks. *Science*. 301:1870–1874.

Liu J, Newsome WT. 2006. Local field potential in cortical area MT: stimulus tuning and behavioral correlations. *J Neurosci*. 26:7779–7790.

Logothetis NK, Pauls J, Augath M, Trinath T, Oeltermann A. 2001. Neurophysiological investigation of the basis of the fMRI signal. *Nature*. 412:150–157.

Lund JS, Angelucci A, Bressloff PC. 2003. Anatomical substrates for functional columns in macaque monkey primary visual cortex. *Cereb Cortex*. 13:15–24.

MacLeod K, Bäcker A, Laurent G. 1998. Who reads temporal information contained across synchronized and oscillatory spike trains? *Nature*. 395:693–698.

Martínez-Trujillo JC, Treue S. 2002. Attentional modulation strength in cortical area MT depends on stimulus contrast. *Neuron*. 35:365–370.

Muthukumaraswamy SD, Singh KD. 2013. Visual gamma oscillations: the effects of stimulus type, visual field coverage and stimulus motion on MEG and EEG recordings. *Neuro Image*. 69:223–230.

Nichols TE, Holmes AP. 2002. Nonparametric permutation tests for functional neuroimaging: a primer with examples. *Hum Brain Mapp*. 15:1–25.

Niessing J. 2005. Hemodynamic signals correlate tightly with synchronized gamma oscillations. *Science*. 309:948–951.

Nolte G. 2003. The magnetic lead field theorem in the quasi-static approximation and its use for magnetoencephalography forward calculation in realistic volume conductors. *Phys Med Biol*. 48:3637–3652.

Oostenveld R, Fries P, Maris E, Schoffelen J-M. 2011. Field trip: open source software for advanced analysis of MEG, EEG, and invasive electrophysiological data. *Comput Intell Neurosci*. 2011:1–9.

Perry G, Hamandi K, Brindley LM, Muthukumaraswamy SD, Singh KD. 2013. The properties of induced gamma oscillations in human visual cortex show individual variability in their dependence on stimulus size. *Neuro Image*. 68: 83–92.

Perry G, Randle JM, Koelewijn L, Routley BC, Singh KD. 2015. Linear tuning of gamma amplitude and frequency to luminance contrast: evidence from a continuous mapping paradigm. *PLoS One*. 10:e0124798.

Ray S, Maunsell JH. 2010. Differences in gamma frequencies across visual cortex restrict their possible use in computation. *Neuron*. 67:885–896.

Rees G, Friston K, Koch C. 2000. A direct quantitative relationship between the functional properties of human and macaque V5. *Nat Neurosci*. 3:716–723.

Rohenkohl G, Bosman CA, Fries P. 2018. Gamma synchronization between V1 and V4 improves behavioral performance. *Neuron*. 100:953, e3–963.

Salinas E, Sejnowski TJ. 2001. Correlated neuronal activity and the flow of neural information. *Nat Rev Neurosci*. 2:539–550.

Scase MO, Braddick OJ, Raymond JE. 1996. What is noise for the motion system? *Vision Res*. 36:2579–2586.

Sclar G, Maunsell JH, Lennie P. 1990. Coding of image contrast in central visual pathways of the macaque monkey. *Vision Res*. 30:1–10.

Siegel M, Donner TH, Engel AK. 2012. Spectral fingerprints of large-scale neuronal interactions. *Nat Rev Neurosci*. 13:121–134.

Siegel M, Donner TH, Oostenveld R, Fries P, Engel AK. 2007. High-frequency activity in human visual cortex is modulated by visual motion strength. *Cereb Cortex*. 17:732–741.

Siegel M, Donner TH, Oostenveld R, Fries P, Engel AK. 2008. Neuronal synchronization along the dorsal visual pathway reflects the focus of spatial attention. *Neuron*. 60:709–719.

Siegel M, König P. 2003. A functional gamma-band defined by stimulus-dependent synchronization in area 18 of awake behaving cats. *J Neurosci*. 23:4251–4260.

Siegel M, Kording KP, König P. 2000. Integrating top-down and bottom-up sensory processing by somato-dendritic interactions. *J Comput Neurosci*. 8:161–173.

Siegel M, Warden MR, Miller EK. 2009. Phase-dependent neuronal coding of objects in short-term memory. *Proc Natl Acad Sci U S A*. 106:21341–21346.

Sohal VS, Zhang F, Yizhar O, Deisseroth K. 2009. Parvalbumin neurons and gamma rhythms enhance cortical circuit performance. *Nature*. 459:698–702.

Tallon-Baudry C, Bertrand O, Delpuech C, Pernier J. 1996. Stimulus specificity of phase-locked and non-phase-locked 40 Hz visual responses in human. *J Neurosci*. 16:4240–4249.

Thut G, Nietzel A, Brandt SA, Pascual-Leone A. 2006. Alpha-band electroencephalographic activity over occipital cortex indexes visuospatial attention bias and predicts visual target detection. *J Neurosci*. 26:9494–9502.

van Kerkoerle T, Self MW, Dagnino B, Gariel-Mathis M-A, Poort J, van der Togt C, Roelfsema PR. 2014. Alpha and gamma oscillations characterize feedback and feedforward processing in monkey visual cortex. *Proc Natl Acad Sci U S A*. 111:14332–14341.

Van Veen BD, Van Drongelen W, Yuchtman M, Suzuki A. 1997. Localization of brain electrical activity via linearly constrained minimum variance spatial filtering. *IEEE Trans Biomed Eng*. 44:867–880.

Vinck M, Bosman CA. 2016. More gamma more predictions: gamma-synchronization as a key mechanism for efficient integration of classical receptive field inputs with surround predictions. *Front Syst Neurosci*. 10:35.

Vinck M, Womelsdorf T, Fries P. 2013. Gamma-band synchronization and information transmission. In: Quiroga RQ, Panzeri S, editors. *Principles of neural coding*. CRC Press, pp. 449–470.

Womelsdorf T, Fries P, Mitra PP, Desimone R. 2006. Gamma-band synchronization in visual cortex predicts speed of change detection. *Nature*. 439:733–736.

Womelsdorf T, Lima B, Vinck M, Oostenveld R, Singer W, Neuenschwander S, Fries P. 2012. Orientation selectivity and noise correlation in awake monkey area V1 are modulated by the gamma cycle. *Proc Natl Acad Sci U S A*. 109:4302–4307.